ACS Photonics

Letter

pubs.acs.org/journal/apchd5

Asymmetric Aluminum Antennas for Self-Calibrating Surface-Enhanced Infrared Absorption Spectroscopy

Benjamin Cerjan,[†] Xiao Yang,[†] Peter Nordlander,[†,§,∥] and Naomi J. Halas*[,†,‡,§,∥]

[†]Department of Physics and Astronomy, [‡]Department of Chemistry, [§]Department of Electrical and Computer Engineering, and [∥]Laboratory for Nanophotonics, Rice University, Houston, Texas 77005, United States

Supporting Information

ABSTRACT: While there has been a tremendous increase of recent interest in noble metal-based antennas as substrates for surface-enhanced infrared absorption spectroscopy, more abundant and manufacturable metals may offer similar or additional opportunities for this mid-infrared sensing modality. Here we examine the feasibility of aluminum antennas for SEIRA, by designing and fabricating asymmetric aluminum cross antennas with nanometer-scale gaps. The asymmetric cross design enables the simultaneous detection of multiple infrared vibrational resonances over a broad region of the mid-infrared spectrum. The presence of the Al_2O_3 amorphous surface oxide layer not only passivates the metal antenna structures but also enables a very straightforward covalent binding chemistry for analyte molecules to the antenna through multiple approaches, in this case by the use of carboxylic acid functional groups. The aluminum−oxygen stretching mode of the oxide can be used as a self-calibration standard to quantify the number of analyte molecules on the antenna surface.

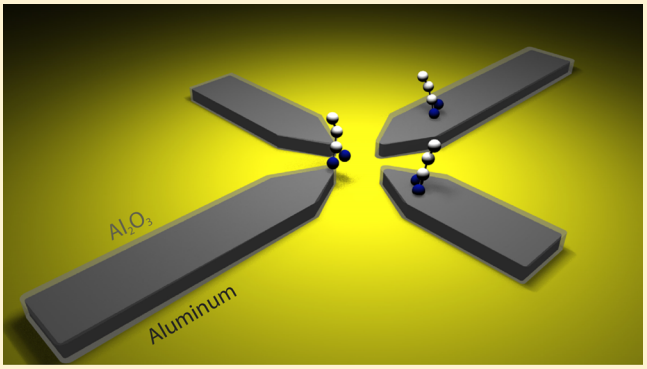

KEYWORDS: *SEIRA, FTIR, aluminum, internal calibration, nanoantenna*

Some of the most promising applications in the field of plasmonics are in surface-enhanced spectroscopies, where metallic nanostructures are designed to provide local electromagnetic field enhancements of adsorbed analyte molecules for chemical detection. In addition to the well-established topics of surface-enhanced Raman scattering (SERS)[1−3] and localized surface plasmon resonance (LSPR) sensing,[4−6] the direct enhancement of vibrational modes of molecules in the infrared "chemical fingerprinting" region of the spectrum, known as surface-enhanced infrared absorption (SEIRA) spectroscopy,[7−12] is a topic of rapidly increasing interest. Unlike SERS and LSPR sensing, which exploit plasmonic effects in the visible and near-IR regions of the spectrum, local field enhancements in the mid-infrared are also enhanced by the lightning-rod effect.[11,13−15] SEIRA antennas have been designed and fabricated in a wide range of geometries,[16−19] and detection of spectroscopic features of molecules deposited on these structures down to zeptomolar concentrations on individual antennas has been reported.[20] These results indicate that the potential for using SEIRA antenna-based substrates for chemical monitoring and identification is quite promising.

While the vast majority of SEIRA-enhancing antennas have been demonstrated using noble metals, the potential of this technique for widespread use with commercial IR spectrophotometers impels us to consider the use of more sustainable and cost-effective materials for this enhanced spectroscopy. Of particular interest is aluminum, which recently has been shown to possess excellent properties for sensing.[21−24] Here we examine the potential of aluminum-based antenna structures for SEIRA. Although the electronic and plasmonic properties of gold and aluminum differ greatly in the visible and UV regions of the spectrum, due to their similarities in the infrared region of the spectrum (see Figure S1), aluminum antennas have been designed, fabricated, and demonstrated as high-quality SEIRA substrates. Asymmetric aluminum cross antennas consisting of two pairs of symmetric arms of two differing lengths, positioned orthogonally with a central nanometer-scale junction gap, support a broad mid-IR resonant response. This geometric arrangement of antennas provides high field enhancement while still supporting two distinct resonances (see Figure S2). This enables the detection of multiple functional groups of an analyte molecule, due to the characteristic coupling of vibrational modes of the molecule to the antenna structure. We observe that while the SEIRA enhancement of Al antennas is somewhat less than what is found for Au antennas of the same geometry, the properties of aluminum provide some unique opportunities as an alternative SEIRA substrate. Specifically, the omnipresent 2−4 nm thick surface oxide layer, which passivates the antenna structure against further oxidation, enables a broader range of covalent binding schemes for molecules to the antenna than Au or Ag. In the present

Received: January 14, 2016
Published: February 14, 2016

DOI: 10.1021/acsphotonics.6b00024
ACS Photonics 2016, 3, 354−360

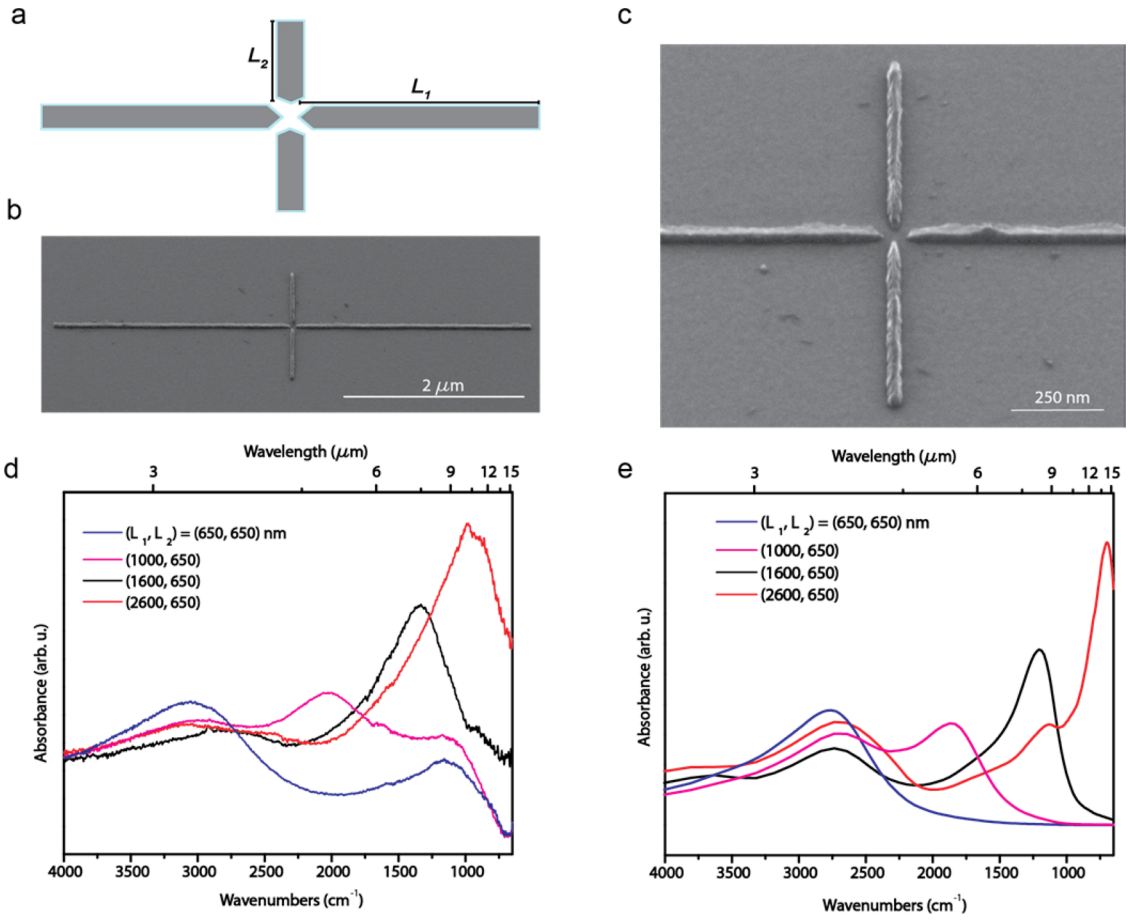

Figure 1. (a) Schematic diagram labeling the variable dimensions of the antenna. L_1 and L_2, the antenna height and width, are fixed at 35 and 50 nm, respectively. (b) High-tilt (75°) SEM image of a single aluminum asymmetric antenna. L_1 and L_2 = 2600 and 650 nm. (c) Increased magnification image showing the surface roughness of the alumina. (d) Tuning of 3 × 3 (9 μm pitch in both directions) arrays of asymmetric Al antennas across the IR "fingerprinting region". The peak at 950 cm^{-1} is due to the native aluminum oxide layer, measured using unpolarized light to excite both arms of the antenna. (e) Simulated absorption spectra of the same antennas in (d).

study we demonstrate functionalization of analyte molecules to the antenna based on their carboxylic (−COOH) functional groups, studying the SEIRA response of stearic acid molecules bound to Al antennas, and are able to observe the characteristics of this substrate−adsorbate binding in detail. By tuning one pair of the antenna arms to be resonant with the dominant aluminum−oxygen stretching mode of the surface oxide, we show that the inherent SEIRA signal from the oxide layer can be used as a self-calibration to monitor relative concentrations of analyte bound to the antenna surface against the Al−O "standard".

An SEM image of the antenna geometry is shown in Figure 1b; Figure 1a displays the corresponding schematic diagram. The asymmetric cross antenna consists of two horizontal Al nanorods with a length L_1 and two vertical nanorods of length L_2. Both pairs of arms taper to a tip with a radius of curvature of ∼6 nm at the central junction, where opposite rods are separated by a gap size of 30 nm. The thickness of the antenna is nominally 35 nm, but in Figure 1c, the surface roughness of the antenna due to the presence of the native aluminum oxide coating is clearly observable. The tapering distance is 75 nm from each tip. The antennas are excited at an incident angle θ, which ranges from 15° to 30°, using unpolarized light. In this study we measure 3 × 3 arrays of antennas to demonstrate the proof-of-concept with readily apparent signal strength. Previous studies have demonstrated that these results should be directly scalable to single-antenna measurements.[20] The antennas are straightforwardly tuned across the IR "fingerprinting" region, as shown in Figure 1d, and correspond to simulated models of these structures, Figure 1e. The prominent dip in the spectra for the experimentally characterized longer antennas (Figure 1d) near 950 cm^{-1} is the ν(Al−O) vibration.[25] The discrepancy between the simulated and experimental antennas at lower energies is due to difficulty in modeling the very thin Al_2O_3 layer on the surface of the antenna, leading to differences near the ν(Al−O) vibration.

To learn more about the properties of asymmetric Al nanoantennas, it is useful to directly compare the same antenna structure made from Al with the same structure made from Au (Figure 2). Here the antenna resonances are tuned to ∼1100 and ∼3000 cm^{-1}, the spectral regions for Al−O vibrations and for C−H molecular vibrations, respectively, by tuning the arm lengths to L_1= 1800 nm and L_2 = 525 nm (Figure 2a). A distinct absorptive shoulder at 950 cm^{-1} can be observed in the spectrum of the Al antenna, which is absent in the Au antenna spectrum. We attribute this shoulder to the presence of the native oxide layer on the Al antenna. In Figure 2b,c we see a direct comparison of the near-field enhancements ($|E|/|E_0|$) in the antenna junction region of both the Au and the Al antennas, calculated using FDTD simulations. The simulations

DOI: 10.1021/acsphotonics.6b00024
ACS Photonics 2016, 3, 354−360

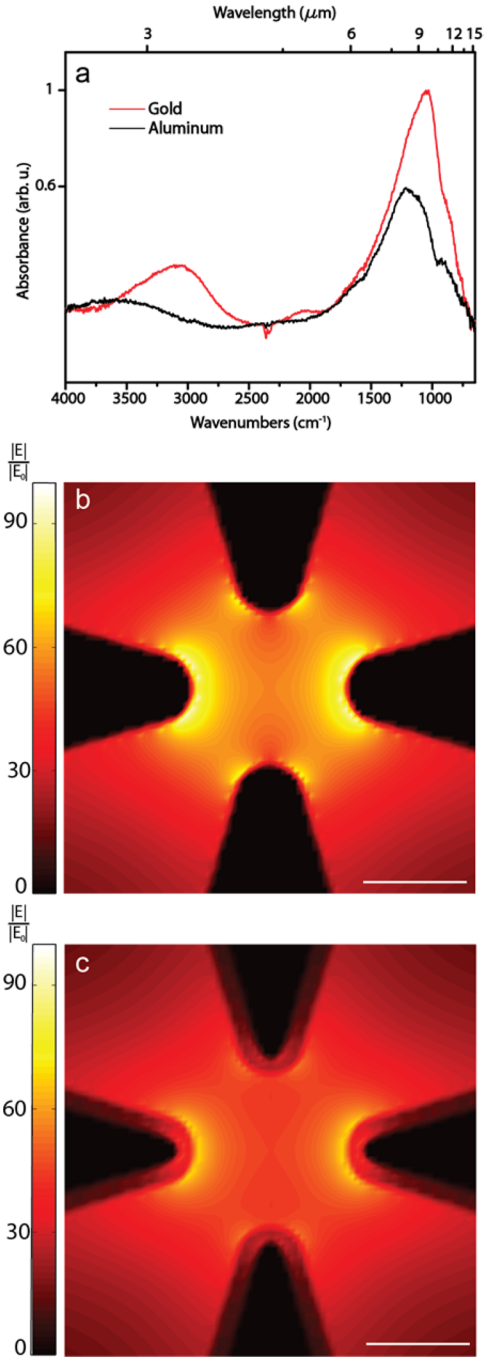

Figure 2. (a) Au and Al 3 × 3 antenna array spectrum comparison for antennas with L_1 and L_2 = 1800 and 525 nm. (b) Simulated peak electric field enhancement for the gold antenna at 2920 cm^{-1}. (c) Simulated peak electric field enhancement for the aluminum antenna at 3185 cm^{-1}. Scale bars in (b) and (c) are 20 nm.

were performed at the wavenumber corresponding to the maximum local electric field enhancement (2920 and 3185 cm^{-1} for Au and Al, respectively). For both structures, the results clearly show that the field enhancements are concentrated in the junction. A direct comparison of these two simulations shows that the local field enhancement is stronger for Au than for Al, due both to the presence of the Al_2O_3 oxide layer for the Al antenna case as well as to the greater loss in the dielectric function of Al in this energy range. However, it is important to point out that the lower field enhancement in Al is not that severe: in this case, we observe a peak field enhancement near 90−95 for Au and in the 55−60 range for Al. While this lower field enhancement factor may make ultrasensitive trace chemical detection with Al nanoantennas slightly less feasible than with Au nanoantennas, the benefits of internal calibration based on the aluminum oxide make aluminum a compelling material for use in future SEIRA studies.

The asymmetric Al antenna design supports a strong SEIRA signal for molecular adsorbates (Figure 3) and also allows for polarization-dependent detection (Figure S3). Because of the Al_2O_3 terminating layer of the antenna, the chemistry for molecular functionalization of Al antennas differs entirely from the largely thiol-based surface functionalization chemistry of Au nanostructures. The oxide layer supports numerous attachment chemistries applicable to a wider variety of functional groups. One such example is the carboxylic acid functional group, which can be bound to the oxide surface layer of the antenna by a straightforward condensation reaction. The functionalization of Al nanoantennas and the SEIRA spectrum of the adsorbate is shown in Figure 3. Here we use stearic acid (also known as octadecanoic acid, $C_{17}H_{35}CO_2H$) as our analyte molecule. It has been shown that stearic acid forms a self-assembled monolayer (SAM) on alumina and that the binding of the carboxylate group with the alumina surface is surprisingly complex, displaying four separate types of binding.[26,27] In Figure 3a, which shows both the nonfunctionalized and the functionalized antenna spectrum, the molecular signal is clearly visible (red curve) as a series of Fano lineshapes superimposed on the broad antenna background. A closer look at the C−H stretching region (Figure 3b) shows the CH_2 symmetric and antisymmetric stretching modes at 2920 and 2850 cm^{-1} as well as the terminal CH_3 group at 2950 cm^{-1}. In the region of the spectrum corresponding to the carboxylic acid stretch modes for the bound adsorbate molecule (Figure 3c), the observed vibrations at 1540 and 1560 cm^{-1} report some of the types of bonding that can occur between a carboxylic acid and an alumina surface; the vibrations at 1592 and 1464 cm^{-1} are due to the CO_2 symmetric stretch and the combination of CO_2 and CH_2 stretch modes, respectively.[27] With these antennas we are able to detect subsets of the total population of binding events at the surface of the antenna, indicating the sensitivity of the device. Were these antennas tuned to more strongly overlap the CO stretching region (∼1400−1600 cm^{-1}), we would expect the sensitivity to these various binding types to improve by approximately a factor of 2.5 (see Figure S4). Better overlap between the resonant energy of the local field enhancement and the molecular vibration of interest would lead to improved molecular detection, but as can be seen from Figure 3a even off-resonant vibrations are still readily detected due to the sensitivity of the device.

To examine how the inherent absorption feature corresponding to the Al_2O_3 capping layer can be utilized to calibrate adsorbate coverage, we prepared antennas with L_1 = 650 and L_2 = 2600 nm. This antenna exhibited a response peak at both the Al_2O_3 resonance and the CH stretching region. We then functionalized a series of antennas by immersion in increasing concentrations of stearic acid. This procedure allows us to obtain an adsorption isotherm for our antenna as a function of analyte solution concentration. As the concentration of stearic acid is increased, the partial pressure of the solute increases, resulting in a greater concentration of stearic acid onto the

DOI: 10.1021/acsphotonics.6b00024
ACS Photonics 2016, 3, 354−360

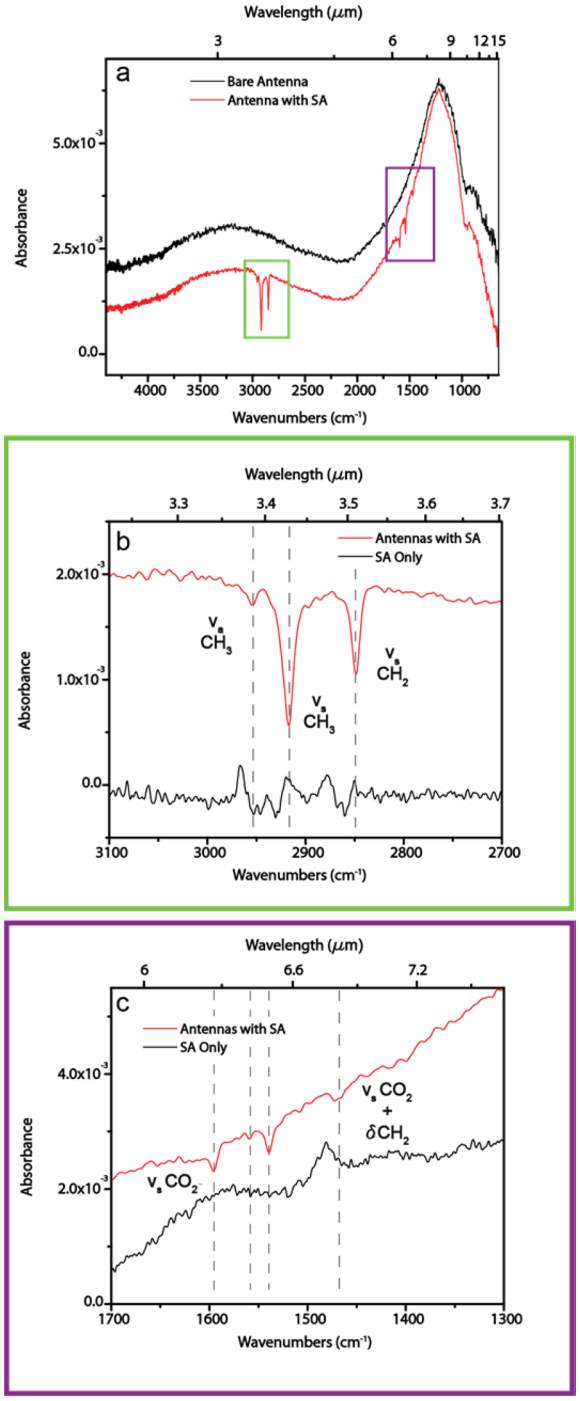

Figure 3. (a) Comparison of spectra from a 3 × 3 Al antenna array (L_1 and L_2 = 1800 and 650 nm) before and after stearic acid (SA) functionalization in a 2 mM solution. (b) Expanded view of the C−H group region molecular signal on the antennas and a reference spectrum of a stearic acid SAM on bulk aluminum film (scaled for visibility), with prominent vibrations at 2850, 2920, and 2950 cm^{-1} labeled. (c) Expanded view of CO vibration region with the vibrations indicated at 1464 and 1592 cm^{-1}, as well as a pair of mixed-strength C−O bonds at 1540 and 1560 cm^{-1}, indicating different types of bonding between the carboylate headgroup and the alumina surface.

junction surfaces of the antennas until total coverage is achieved.

To extract the peak strengths of the various molecular vibrations, we first performed asymmetric least-squares smoothing (AsLSS) on the data, shown in Figure S5.[28] This removed the "background" antenna signal from the spectrum and resulted in spectra such as those in Figure 4b,c,d. Then we fit the resulting absorbance spectrum, $A(\omega)$, with a summation of Fano functions for the C−H region, as shown by the solid lines in Figure 4b,c,

$$A(\omega) = b + a_1\frac{\left(q_1\frac{\Gamma_1}{2} + \omega - \omega_{r_1}\right)^2}{\left(\frac{\Gamma_1}{2}\right)^2 + (\omega - \omega_{r_1})^2} + a_2\frac{\left(q_2\frac{\Gamma_2}{2} + \omega - \omega_{r_2}\right)^2}{\left(\frac{\Gamma_2}{2}\right)^2 + (\omega - \omega_{r_2})^2} \quad (1)$$

where b is a constant to account for any background offset and a_i is the strength; q_i is the Fano parameter; Γ_i is the damping; and ω_{r_i} is the resonant frequency of the ith vibration (i = 1, 2). Similarly, for the Al_2O_3 vibration we use only a single Fano function (a_2 = 0), as shown by the solid line in Figure 4d. This simple fitting function is based on a more rigorous quantum mechanical description that accounts for various combinations of substrate−analyte interaction strengths and symmetries to produce both asymmetric and "spike" lineshapes.[29] The inclusion of a strength parameter "a_i" allows us to determine the relative amplitudes of the molecular peaks in the antenna spectrum. It should be noted that this model works equally well for both large well-defined "spikes" (Figure 4b) and less intense asymmetric lineshapes (Figure 4c). These different lineshapes at low concentration could be due to a large number of effects, such as surface defects on the antenna or slight differences in antenna−adsorbate interactions, producing different coupling between the antenna and the SAM. This method is even able to detect peaks only marginally above the noise floor of the spectrometer used, as evidenced by the substantial noise surrounding the peaks in Figure 4b,c. By computing the Fano peak ratio (FPR) for these resonances,

$$\mathrm{FPR} \equiv \frac{|a_{\nu_a-CH_2}| + |a_{\nu_s-CH_2}|}{a_{Al_2O_3}} \quad (2)$$

we are able to determine the ratio of the "strength" of the C−H group peaks to that of the Al_2O_3 peak, for a given concentration. Note that we must compare the summation of the two peak strengths since the tails of the first resonance contribute to the peak height of the second resonance and vice versa.

By assuming that the amorphous Al_2O_3 layer on the surface of the antenna is composed of a similar number of bonds between different antennas, we can use the "strength" of the Al_2O_3 vibrational reference as an internal standard. By comparing the signal intensity of the C−H stretches with that of the Al_2O_3 stretch, we are able to determine the FPR (eq 2), an extrinsic quantity independent of the particular antenna(s) being measured. By comparing FPR, as opposed to absolute signal intensity, we are able to account for differences in junction field intensity arising from slight antenna-to-antenna variations in junction geometry. A larger FPR corresponds to higher molecular coverage on the junction surfaces of the antenna, as the strength of the C−H vibrations grows relative to the reference of the Al_2O_3 vibration. Another potential use of this analysis is the ability to probe and quantify the variations between antennas by focusing on the absolute

DOI: 10.1021/acsphotonics.6b00024
ACS Photonics 2016, 3, 354−360

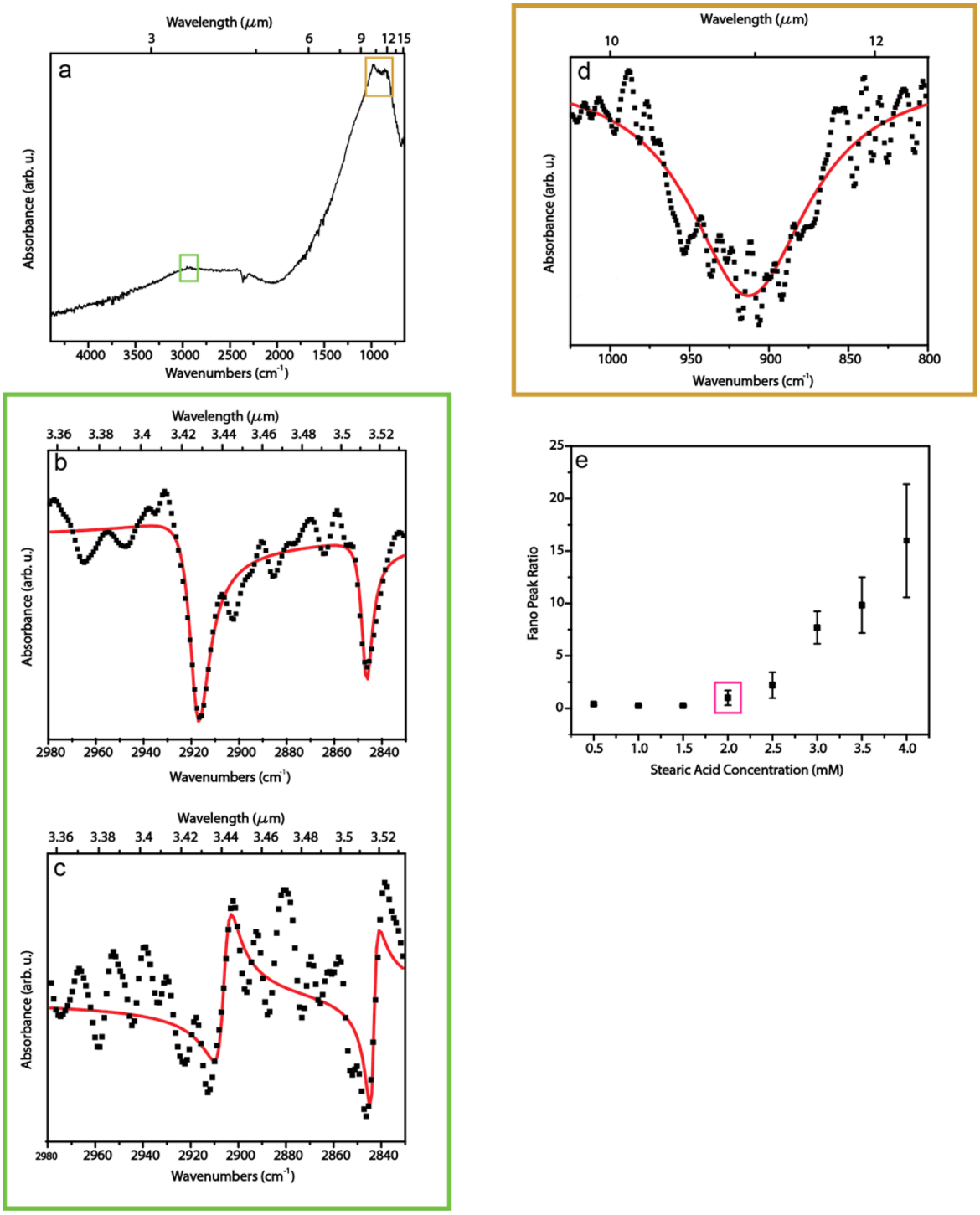

Figure 4. (a) Full spectrum of a 3 × 3 antenna array functionalized in 2.0 mM stearic acid solution. (b) Fitting of a double Fano function for the C−H peaks with "spike" molecular signals. (c) Double Fano peak approximation after immersion with asymmetric molecular signals. (d) Single Fano peak approximation for Al−O vibration. (e) Concentration dependence of the molecular signal by comparing the strength of the Al_2O_3 resonance with that of the symmetric and asymmetric CH_2 vibrations; see eq 2. Error bars indicate the SD from three sets of antennas that underwent the same immersion steps. The immersion concentration used for detection in (a), (b), and (c) is indicated in magenta.

strength of the Al_2O_3 vibration, below the resolution limit of traditional near-field optics.

Using the FPR as a stand-in for molecular coverage we can plot a simple isotherm for our antenna−molecule system, as shown in Figure 4e. Note that the results become less repeatable as the concentrations increase (error bars are from three separate sets of antenna measurements), even though all measured antennas were immersed in the same solution for the same amount of time. We believe this to be the result of the irreproducibility in SAM formation as a result of surface defects.[30] As the measured volume decreases to the nanoscale, we would expect the surface roughness of the antennas (Figure 1c) to play an even larger role than previously reported for large-area films (Figure S6). Additionally, at higher concen-

DOI: 10.1021/acsphotonics.6b00024
ACS Photonics 2016, 3, 354−360

trations the background measurements become increasingly erratic, leading to relatively large systematic error in the high-concentration measurements, effectively masking the saturation of the isotherm. We speculate that this is due to aggregates of stearic acid assembling on the substrate due to their strong intermolecular van der Waals forces, leading to the substantial variation in FPR at higher concentrations.

These results demonstrate the ability of this system to quantify the number of molecules on the antenna, relative to the internal standard of the Al_2O_3 vibration. For a completely covered antenna we would expect there to be $\sim 3.6 \times 10^4$ molecules in the tip region of the antenna, based on the footprint of stearic acid.[30] By scaling this number down based on the relative peak heights, we find that our antennas are sensitive to ~4000 molecules of stearic acid (deposited at 2.0 mM concentration). Note that the peaks for incomplete SAMs may overestimate the number of molecules present, as the molecules are able to bend over to allow the long carbon chain to become closer to the antenna junction surface where the electric field enhancement is greater, increasing the strength of the C−H vibrations.

Using this approach, aluminum antennas can be used to simultaneously detect and quantify the molecules present on their junction surfaces based purely on IR measurements calibrated to their own internal standard. Additionally, this method can be used to extract chemical information about the types of binding occurring at the surface of the antenna. This technique demonstrates how these structures are able to measure and extract relevant information about a target molecule on the surface of the antenna, including the detailed vibrational spectrum with its structural information and the number of molecules on the antenna.

In conclusion, we have shown that asymmetric Al antennas provide a novel device design for quantitative SEIRA. With this geometry, it is possible to measure the vibrational resonances of both the native oxide on the Al antennas and a target molecule of interest. The native Al_2O_3 layer on the antennas serves as a reference measurement for determining the number of molecules present on the antenna. Due to the high sensitivity of the antennas, complex molecular bond information can also be extracted. This work demonstrates the feasibility for high-quality SEIRA spectroscopy measurements with highly abundant and low-cost metallic antenna structures.

■ ASSOCIATED CONTENT

Supporting Information

The Supporting Information is available free of charge on the ACS Publications website at DOI: 10.1021/acsphotonics.6b00024.

Detailed descriptions of the sample fabrication, the experimental setup, sample characterization and analysis, and the theoretical methods. (PDF)

■ AUTHOR INFORMATION

Corresponding Author

*E-mail: halas@rice.edu

Notes

The authors declare no competing financial interest.

■ ACKNOWLEDGMENTS

N.J.H. and P.N. acknowledge support from the Robert A. Welch Foundation under grants C-1220 and C-1222, the Army Research Office under grant W911NF-12-1-0407, and the Defense Threat Reduction Agency under grant HDTRA1-11-1-0040.

■ REFERENCES

(1) Moskovits, M. Surface-Enhanced Spectroscopy. *Rev. Mod. Phys.* **1985**, *57*, 783.

(2) Zrimsek, A. B.; Henry, A.; Van Duyne, R. P. Single Molecule Surface-Enhanced Raman Spectroscopy without Nanogaps. *J. Phys. Chem. Lett.* **2013**, *4*, 3206−3210.

(3) Le Ru, E. C.; Etchegoin, P. G. Single-Molecule Surface-Enhanced Raman Spectroscopy. *Annu. Rev. Phys. Chem.* **2012**, *63*, 65−87.

(4) Willets, K. A.; Van Duyne, R. P. Localized Surface Plasmon Resonance Spectroscopy and Sensing. *Annu. Rev. Phys. Chem.* **2007**, *58*, 267−297.

(5) Mayer, K. M.; Hafner, J. H. Localized Surface Plasmon Resonance Sensors. *Chem. Rev.* **2011**, *111*, 3828−3857.

(6) Anker, J. N.; Hall, W. P.; Lyandres, O.; Shah, N. C.; Zhao, J.; Van Duyne, R. P. Biosensing with Plasmonic Nanosensors. *Nat. Mater.* **2008**, *7*, 442−453.

(7) Pucci, a.; Neubrech, F.; Weber, D.; Hong, S.; Toury, T.; de la Chapelle, M. L. Surface Enhanced Infrared Spectroscopy Using Gold Nanoantennas. *Phys. Status Solidi B* **2010**, *247*, 2071−2074.

(8) Brown, L. V.; Zhao, K.; King, N.; Sobhani, H.; Nordlander, P.; Halas, N. J. Surface-Enhanced Infrared Absorption Using Individual Cross Antennas Tailored to Chemical Moieties. *J. Am. Chem. Soc.* **2013**, *135*, 3688−3695.

(9) Adato, R.; Altug, H. In-Situ Ultra-Sensitive Infrared Absorption Spectroscopy of Biomolecule Interactions in Real Time with Plasmonic Nanoantennas. *Nat. Commun.* **2013**, *4*, 2154.

(10) Aksu, S.; Cetin, A. E.; Adato, R.; Altug, H. Plasmonically Enhanced Vibrational Biospectroscopy Using Low-Cost Infrared Antenna Arrays by Nanostencil Lithography. *Adv. Opt. Mater.* **2013**, *1*, 798−803.

(11) Le, F.; Brandl, D. W.; Urzhumov, Y. a; Wang, H.; Kundu, J.; Halas, N. J.; Aizpurua, J.; Nordlander, P. Metallic Nanoparticle Arrays: A Common Substrate for Both Surface-Enhanced Raman Scattering and Surface-Enhanced Infrared Absorption. *ACS Nano* **2008**, *2*, 707−718.

(12) Abb, M.; Wang, Y.; Papasimakis, N.; De Groot, C. H.; Muskens, O. L. Surface-Enhanced Infrared Spectroscopy Using Metal Oxide Plasmonic Antenna Arrays. *Nano Lett.* **2014**, *14*, 346−352.

(13) Yin, L.; Vlasko-Vlasov, V. K.; Pearson, J.; Hiller, J. M.; Hua, J.; Welp, U.; Brown, D. E.; Kimball, C. W. Subwavelength Focusing and Guiding of Surface Plasmons. *Nano Lett.* **2005**, *5*, 1399−1402.

(14) Bochterle, J.; Neubrech, F.; Nagao, T.; Pucci, A. Angstrom-Scale Distance Dependence of Antenna-Enhanced Vibrational Signals. *ACS Nano* **2012**, *6*, 10917−10923.

(15) Ermushev, A. V.; Mchedlishvili, B. V.; Oleynikov, V. A.; Petukhov, A. V. Surface Enhancement of Local Optical Fields and the Lightning-Rod Effect. *Quantum Electron.* **1993**, *23*, 435−440.

(16) Chen, K.; Adato, R.; Altug, H. Dual-Band Perfect Absorber for Multispectral Plasmon-Enhanced Infrared Spectroscopy. *ACS Nano* **2012**, *6*, 7998−8006.

(17) Aouani, H.; Šípová, H.; Rahmani, M.; Navarro-Cia, M.; Hegnerová, K.; Homola, J.; Hong, M.; Maier, S. a. Ultrasensitive Broadband Probing of Molecular Vibrational Modes with Multifrequency Optical Antennas. *ACS Nano* **2013**, *7*, 669−675.

(18) Neubrech, F.; Weber, D.; Enders, D.; Nagao, T.; Pucci, A. Antenna Sensing of Surface Phonon Polaritons. *J. Phys. Chem. C* **2010**, *114*, 7299−7301.

(19) Landy, N. I.; Sajuyigbe, S.; Mock, J. J.; Smith, D. R.; Padilla, W. J. Perfect Metamaterial Absorber. *Phys. Rev. Lett.* **2008**, *100*, 207402.

(20) Brown, L. V.; Yang, X.; Zhao, K.; Zheng, B. Y.; Nordlander, P.; Halas, N. J. Fan-Shaped Gold Nanoantennas above Reflective Substrates for Surface-Enhanced Infrared Absorption (SEIRA). *Nano Lett.* **2015**, *15*, 1272−1280.

DOI: 10.1021/acsphotonics.6b00024
ACS Photonics 2016, 3, 354−360

(21) King, N. S.; Liu, L.; Yang, X.; Cerjan, B.; Everitt, H. O.; Nordlander, P.; Halas, N. J. Fano Resonant Aluminum Nanoclusters for Plasmonic Colorimetric Sensing. *ACS Nano* **2015**, *9*, 10628.
(22) Tan, S. J.; Zhang, L.; Zhu, D.; Goh, X. M.; Wang, Y. M.; Kumar, K.; Qiu, C. W.; Yang, J. K. W. Plasmonic Color Palettes for Photorealistic Printing with Aluminum Nanostructures. *Nano Lett.* **2014**, *14*, 4023−4029.
(23) Zhu, X.; Vannahme, C.; Højlund-Nielsen, E.; Mortensen, N. A.; Kristensen, A. Plasmonic Colour Laser Printing. *Nat. Nanotechnol.* **2015**, 1−6.
(24) Duempelmann, L.; Casari, D.; Luu-Dinh, A.; Gallinet, B.; Novotny, L. Color Rendering Plasmonic Aluminum Substrates with Angular Symmetry Breaking. *ACS Nano* **2015**, *9*, 12383−12391.
(25) Van den Brand, J.; Blajiev, O.; Beentjes, P. C. J.; Terryn, H.; de Wit, J. H. W. Interaction of Anhydride and Carboxylic Acid Compounds with Aluminum Oxide Surfaces Studied Using Infrared Reflection Absorption Spectroscopy. *Langmuir* **2004**, *20*, 6308−6317.
(26) Pertays, K. M.; Thompson, G. E.; Alexander, M. R. Self-Assembly of Stearic Acid on Aluminium: The Importance of Oxide Surface Chemistry. *Surf. Interface Anal.* **2004**, *36*, 1361−1366.
(27) Lim, M.; Feng, K.; Chen, X.; Wu, N. Adsorption and Desorption of Stearic Acid Self-Assembled Monolayers on Aluminum Oxide. *Langmuir* **2007**, *23*, 2444−2452.
(28) Eilers, P. H. C. A Perfect Smoother. *Anal. Chem.* **2003**, *75*, 3631−3636.
(29) Langreth, D. C. Energy Transfer at Surfaces: Asymmetric Line Shapes and the Electron-Hole-Pair Mechanism. *Phys. Rev. Lett.* **1985**, *54*, 126−129.
(30) Allara, D. L.; Nuzzo, R. G. Spontaneously Organized Molecular Assemblies. 1. Formation, Dynamics, and Physical Properties of N-Alkanoic Acids Adsorbed from Solution on an Oxidized Aluminum Surface. *Langmuir* **1985**, *1*, 45−52. Allara, D. L.; Nuzzo, R. G. Spontaneously Organized Molecular Assemblies. 2. Quantitative Infrared Spectroscopic Determination of Equilibrium Structures of Solution-Adsorbed N-Alkanoic Acids on an Oxidized Aluminum Surface. *Langmuir* **1985**, *1*, 52−66.

DOI: 10.1021/acsphotonics.6b00024
ACS Photonics 2016, 3, 354−360